Materials Today Chemistry 42 (2024) 102359

Contents lists available at ScienceDirect

Materials Today Chemistry

journal homepage: www.journals.elsevier.com/materials-today-chemistry/

Hydrogenation of graphene on Ni(111) by H_2 under near ambient pressure conditions

Giovanni Carraro [a], Sina Ebrahim Atakoohi [b], Daniele Perilli [d], Ola Alayan [c], Gianangelo Bracco [a,c], Gabriella Garbarino [b], Paul M. Leidinger [e], Zbynek Novotny [e,1], Mario Rocca [a,c], Letizia Savio [a], Marco Smerieri [a], Cristiana Di Valentin [d], Luca Vattuone [a,c,*]

[a] IMEM-CNR Unità di Genova, Via Dodecaneso 33, 16146, Genova, Italy
[b] DICCA Università di Genova, Via Opera Pia, 16145, Genova, Italy
[c] DIFI Università di Genova, Via Dodecaneso 33, 16146, Genova, Italy
[d] Department of Materials Science, University of Milano-Bicocca, Via R. Cozzi 55, I-20125, Milano, Italy
[e] Swiss Light Source, Paul Scherrer Institute, Forschungsstrasse 111, 5232, Villigen, Switzerland

A B S T R A C T

Graphene hydrogenation on Ni(111) in the mbar region has been investigated by combining Near Ambient Pressure X-ray Photoemission Spectroscopy and Density Functional Theory calculations. A complete and nearly perfect graphene single layer and an incomplete defective monolayer were exposed to a methanation mixture (H_2 + CO and H_2 + CO_2, respectively) with a large excess of H_2. The observed behavior is quite different for the two systems. In the former case, the C 1s spectrum of the initially strongly interacting graphene shows the appearance of new components corresponding to hydrogenated C atoms and their first nearest neighbors. The defective carbon layer, grown in the presence of sulfur contamination and consisting of a mixture of strongly and weakly interacting graphene with a significant amount of dissolved C, initially shows the same C species and then evolves with the formation of sp^3 carbon and patches of Ni oxide/hydroxide. NiO forms by CO_2 dissociation, while sp^3 carbon is indicative of a rumpling of the graphene adlayer induced by hydrogenation. Both species disappear when annealing in H_2. Dissociation of H_2 and graphene hydrogenation is possible thanks to the presence of the Ni substrate which makes the reaction weakly exothermic and significantly reduces the barrier for H_2 dissociation.

1. Introduction

The graphene/Nickel (G/Ni) system is characterized by a strong interaction with the substrate, that causes a modification of the G electronic structure and the non-preservation of the Dirac cone at the K point [1]. Despite this, the G/Ni interface has been widely studied over the past decades; the interest is motivated, e.g., by the possible use of G as protective layer [2] as well as for confined chemistry [3,4]. On the one hand, the corrosion resistance of G-covered Ni is twenty times higher than that of bare Ni, while G-covered Cu is seven times more resistant than bare Cu [5]. The former system is a paradigmatic case for strong interaction with a reduced C–Ni distance and a significant rehybridization. At the same time, the latter is the most common example of weak interaction with a relatively large distance between the G adlayer and the Cu substrate.

The G/metal interface determines critically the performance of G coatings, and strong chemical G/metal binding has been found to increase the stability and lubricating performance of G for various metal substrates [6]. On the other hand, it has been recently shown that the confinement of reactants under monolayer cover (such as G or boron nitride) can lead to enhanced reactivity [3]. Reactions such as CO oxidation may then occur at lower temperature thanks to the reduction of the activation barrier due to the energetic cost of the intercalation of the reactants under the cover [3,7]. Such cost is expected to be higher for strongly interacting G, and, indeed, some of us reported recently CO intercalation [8,9] and the occurrence of the Boudouard reaction [4] under G cover on Ni(111). Ni is an important catalyst for several industrial reactions due to its high reactivity and moderate cost [10–12]. In particular, in this research, we focus our interest on the energetically relevant CO_2 methanation reaction, for which intercalation of the reactants under G cover is required.

To this purpose, G grown on Ni(111) has been exposed to a H_2/CO

* Corresponding author. IMEM-CNR Unità di Genova, Via Dodecaneso 33, 16146, Genova, Italy.
E-mail address: luca.vattuone@unige.it (L. Vattuone).
[1] Present address: Physical and Computational Sciences Directorate and Institute for Integrated Catalysis, Pacific Northwest National Laboratory, Richland, WA 99352, USA.

https://doi.org/10.1016/j.mtchem.2024.102359
Received 12 July 2024; Received in revised form 27 September 2024; Accepted 12 October 2024
Available online 22 October 2024

(or H_2/CO_2) mixture in strong excess of H_2, i.e. under conditions mimicking those for which the methanation reaction is performed. CO has thereby been delivered on purpose while exposure to CO_2 occurred due to contamination of H_2 in the Near Ambient Pressure experiments.

We compare the behavior of a pure and complete strongly interacting G monolayer (G^C in the following) to the one of a mixture of strongly and weakly interacting G obtained by growing the film in the presence of S contamination (G^S in the following), where S is a well-known undesired poison for the methanation reaction [13–15]. The former condition (G^C) corresponds to a prototypical investigation of a well-characterized model system widely used for studying intercalation and confined reactions. The latter (G^S) is necessarily less well defined but closer to the conditions present in a real catalytic reactor, where it is not unusual to have some C in the bulk of the catalyst and traces of S at its surface. The amount of C in the bulk severely affects the nature of the carbon species at the surface. At the same time S-contamination modifies the activity of the catalyst, typically by inhibiting CO adsorption [13] and dissociation [16] and thus suppressing the methanation activity of Ni Therefore, S contamination is an issue in the use of biofuel, whereby the removal of sulfur-containing compounds from biogas is mandatory to avoid catalyst deactivation [15,17]. Indeed, the presence of sulfur compounds strongly decreases activity by blocking nickel sites, significantly lowering the hydrogenation rate and affecting the long-term performance of the catalyst [18]. S poisoning of Ni catalysts cannot be avoided in industrial CO_2 methanation reactors. As a general understanding, sulfur reduces the ability of Nickel to adsorb and dissociate H_2, as well as the H spillover capacity, which inhibits the complete hydrogenation of CO* and the formation of CH_4. Additionally, sulfur strengthens the adsorption of the H_3CO* intermediate by accumulating electrons in the bonding region, which increases the energy barrier for the hydrogenation of H_3CO* to CH_4. This favors the production of CO via the decomposition of formate species. The strong chemisorption of sulfur on the Ni surface prevents further adsorption of reactant molecules.

As outlined a long time ago the effect of S on the interaction between Ni and hydrocarbons is quite complex and coverage dependent [19]: for low (4–50 ppm) S content, carbon filament growth is favored while higher S concentration results in formation of 2D or 3D nickel sulfide inhibiting the catalytic activity.

S contamination can also affect graphene growth due to the repulsive interaction between S and C as shown for graphene growth on Ni(110) [20] and for hydrocarbon decomposition on Ni foils [21]. Recently, it has also been shown by theoretical studies that sulfur weakens the interaction between graphene and Fe(111) [22] by changing the graphene-substrate interaction from a strong to a weaker one with an increase in the graphene surface distance and affecting the growth of carbon nanotubes (CNT) on Fe.

On the other hand, the adsorption of an ordered S-layer on Ni(110) was exploited to control the shape of graphene flakes produced by C segregation [23] since the surface sites occupied by S block the growth of the graphene domains [22].

In a broader context, the interaction of H_2 with graphene is a topic of interest by itself [24–26], and the present study fills up the gap between fundamental studies employing atomic H or D and more applied conditions where ambient or near ambient H_2 pressure is used [27]. In fact, while exposure to atomic H promptly leads to G hydrogenation, high pressure is required if molecular H_2 is used [28,29]. We show here that a reactive substrate such as Ni(111) significantly reduces the activation barrier for direct G hydrogenation [30]. Moreover, when exposing G/Ni to H_2 in the mbar regime, both direct hydrogenation of G on the vacuum side and intercalation of H_2 under G followed by dissociation become possible. The former process is due to H_2 dissociation, and it is favored by the presence of defects.

2. Materials and methods

2.1. Experimental methods

The G^C experiment has been performed at the TEMPO beamline of the SOLEIL Synchrotron Radiation source (Saint-Aubin, France) [31] with the Near Ambient Pressure X-Ray Photoemission Spectroscopy (NAPXPS) facility of Sorbonne Université. The experimental setup is described in detail in Ref. [31] and in our previous studies [4,32]. The G^S experiments were performed at the in-situ Spectroscopy beamline of the Swiss Light Source (SLS) at the Paul Scherrer Institute (PSI), also hosting a NAP-XPS facility [33].

In both cases, the Ni(111) sample is cleaned in the preparation chamber by sputtering and annealing cycles following the usual procedure reported in Ref. [34], while graphene is grown by segregation of dissolved carbon (G^C) or by exposure to C_2H_4 following the recipe given in Ref. [34] (G^S).

In the preparation chamber, the sample can be annealed up to 1270 K by electron bombardment while, in the main chamber, it can be heated up to 670 K by a ceramic button heater.

High-purity H_2 gas (purity >99.99 %) is introduced into the analysis chamber through a gas mixer. The pressure in the chamber is read by a cold-cathode ion gauge in the high vacuum limit and by a capacitive gauge for pressures above 5×10^{-4} mbar. Depending on the gas used and on the photoelectron energy of interest, it is possible to perform experiments under NAP at pressures up to 2 mbar. The purity of the gases is checked in the second differential pumping stage of the XPS analyzer by quadrupole mass spectroscopy. In the G^S experiment, hydrogen was slightly contaminated by H_2O and CO_2 impurities (estimated to be ~0.1 % of the H_2 partial pressure) during the transit in the gas-mixing line.

The photon beam impinges at an angle of 54° (G^C) or 60° (G^S) from the surface normal and illuminates a spot of approx. 0.3 mm diameter on the sample. The photoemitted electrons are collected, respectively, at an angle of 0° (G^C) or 30° (G^S) from the surface normal through a nozzle (0.5 mm) leading to the electron energy analyzer (SPECS for GC and Scienta R4000 HiPP-2 for G^S). The angle between the direction of the impinging photons and the one of the emitted electrons is 54° (G^C) or 90° (G^S). The distance between the sample and the nozzle is obtained by optimizing the signal and is typically around 0.6–1.0 mm.

Spectra were recorded at a photon energy $h\nu = 650$ eV (C 1s and O 1s lines) in the G^C experiment and at $h\nu = 742$ eV (O 1s, C 1s, S 2p lines) or $h\nu = 1065$ eV (Ni 2p line) in the G^S experiment. The pass energy was set to 50 eV when recording the C 1s, O 1s, and S 2p regions and to 20 eV for Ni 2p. The energy scale was calibrated on the Fermi edge of the corresponding spectrum. The obtained spectra were normalized on the low binding energy side of each region to allow for a straightforward comparison.

The spectra are analyzed using the Kol-XPD software [35]. After subtracting a Shirley background, a Doniach Sunjic line shape was used to fit the C 1s component of graphene, while a Voigt line shape was used for all the other C 1s components and the O 1s and S 2p ones. In the fits, the position of the peaks was allowed to shift by ±0.1 eV with respect to the reference value shown in the figures.

For GS the highest pressure used in the present experiment is ~ 1.5 mbar of H_2 with only sub-percentage traces of CO_2 and H_2O. The attenuation of the C 1s and O 1s lines as a function of H_2 pressure was determined by plotting the total O1s and C1s area vs increasing H_2 pressure at RT and assuming a linear behavior (See Fig. S1_GS in Supporting information).

2.2. Theoretical methods

Density Functional Theory (DFT) calculations were performed using the plane-wave-based Quantum ESPRESSO package (QE) [36,37]. The ultrasoft pseudopotentials [38] were adopted to describe the

electron-ion interaction with Ni (3d, 4s), C (2s, 2p), and H (1s), treated as valence electrons. Energy cutoffs of 46 Ry and 326 Ry (for kinetic energy and charge density expansion, respectively) were adopted for all calculations. To properly take into account weak interactions, which are crucial for an accurate description of the graphene/metal interface interaction, the van der Waals density functional vdW-DF2^{C09x} was used [39,40] which has been proven to accurately predict the adsorption geometries and electronic properties of graphene on metal (111) surfaces, in agreement with existing experimental data [39,41]. This approach has been successfully applied in several previous works by us to model different types of graphene/metal interfaces [42,43] as well as other types of interfaces involving other 2D materials/metal surfaces [44] or graphene/aromatic molecules [45]. Spin polarization was always included.

For the simulation of the graphene/Nickel (111) system (G/Ni), we used a commensurate model (keeping the Ni lattice parameter) by interfacing a (3x3) supercell of G on top of a (3x3) supercell of Ni (111), wherein C atoms are placed in both top and fcc positions relative to the Ni(111) substrate. This strongly interacting interface model has been previously employed by some of us [9,46], yielding good agreement when compared to experimental measurements.

The geometry relaxation was performed with a 6 × 6 × 1 Monkhorst-Pack [47] k-points mesh. The Ni(111) surface was modeled by a three-layer slab with a bottom layer fixed to the bulk positions during the geometry relaxation to mimic a semi-infinite solid. To avoid interactions between adjacent periodic images, a vacuum space of about 20 Å in the direction perpendicular to the surface was used, together with a dipole correction. Ball-and-stick models were rendered with VESTA software [48]. Atomic charges were computed using the Bader scheme [49].

The H adsorption energies (ΔE_H), as normalized by the number of H atoms (n), were calculated as follows:

$$\Delta E_H = \frac{E_{nH/system} - \frac{n}{2}{}^{*}E_{H2} - E_{system}}{n}$$

where $E_{nH/system}$ is the total energy of the hydrogenated system with n adsorbed H atoms, E_{H2} is the total energy of an isolated H_2 molecule in the gas phase, and E_{system} is the total energy of the optimized system without any adsorbed H atom.

The Climbing Image−Nudged Elastic Band (CI−NEB) method [50] was employed to simulate the H_2 dissociation process on free-standing G or Ni(111) supported G, generating the minimum energy path of the reaction step and an evaluation of the energy barrier.

The XPS spectra of hydrogenated G/Ni systems were calculated using the ΔSCF approach [51]. This method uses a pseudopotential generated with a full core hole for each ionized inequivalent carbon atom and employs the calculation of relative changes of binding energies, the so-called core-level shifts (CLSs). To enable comparison between CLSs of different configurations (i.e. number and position of H atoms), which are inserted into separated supercells, we have included into each system a single CH_4 molecule, at a distance of 20 Å from the surface, which minimizes their mutual interaction, to act as a reference. This methodology has proven successful in our prior works for calculating XPS spectra [9,46].

3. Results

3.1. Experimental results

The outcome of the experiment performed on a complete G monolayer grown on Ni(111) by C segregation from the bulk (G^C experiment) is reported in Fig. 1. The C 1s spectrum of the as-grown sample (spectrum I – right panel) is characterized by a main peak at 284.7 eV and a low intensity one at 283.4 eV. They are assigned to strongly interacting G and to Ni_2C, respectively.

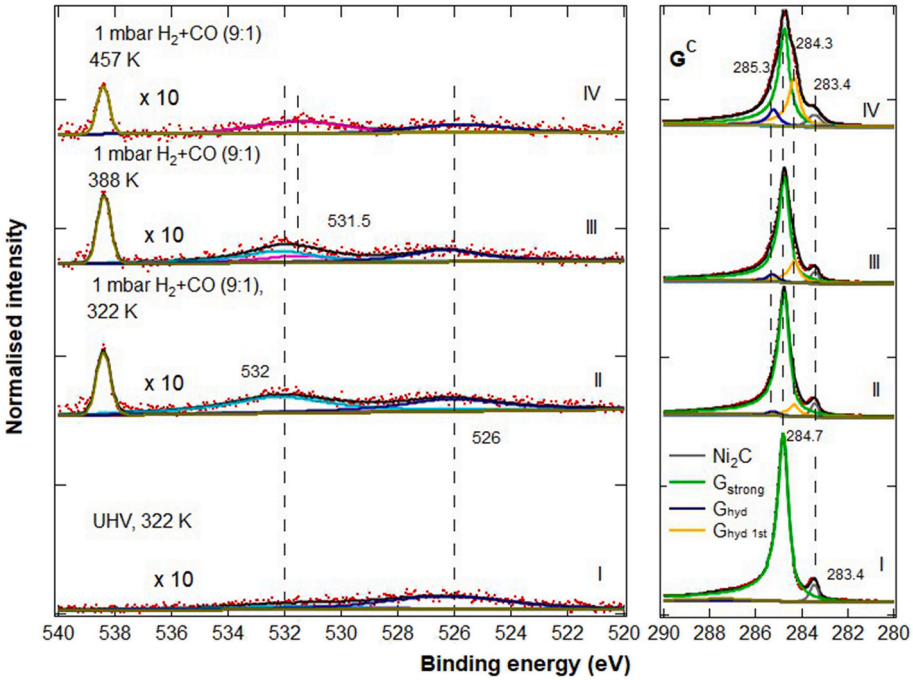

Fig. 1. G^C experiment at Soleil: Hydrogenation of a closed single layer graphene by H_2 exposure. C 1s (right panel) and O 1s (left panel) spectra. Spectrum I corresponds to the condition before exposure to H_2 under UHV; spectra II, III and IV were recorded while exposing the sample to the (9:1) H_2/CO mixture at a total pressure of 1 mbar at 322 K, 388 K, and 457 K, respectively. Spectrum II started after 15 min exposure to the reaction mixture at 322 K; at the end of spectrum II, the temperature is increased while exposing for further 20 min and spectrum III was started when the sample reached 388 K. At the end of spectrum III temperature was raised to 457 K while recording spectra (not shown). Spectrum IV was recorded once the final temperature was reached. Each spectrum requires about 5 min to be recorded during which time the temperature has been kept constant.

Upon exposure of the sample to a H_2:CO = 9:1 mixture at 1 mbar and 322 K, the C 1s main feature broadens (spectrum II) due to the appearance of critical additional components at 285.3 eV and 284.3 eV. Their weight increases when annealing to 388 K (spectrum III) and 457 K (spectrum IV) while exposing the sample to the same mixture. The 284.3 eV peak is usually assigned to weakly interacting G (also addressed as free G): it corresponds to G above surface carbide [9], but it forms also upon CO intercalation in the absence of carbide [52]. Some of us suggested that it might be due to C atoms at the edges of graphene bubbles [4] since a close BE value was previously reported for G above Ar bubbles [53]. Although we postpone the assignment of the different C 1s components to the discussion section, we can already rule out a detachment of G caused by CO intercalation, since deintercalation of this gas is expected around 353 K [52]. Moreover, if CO molecules were present, a correlation would be expected between the intensities of the additional carbon peaks and the O 1s component at 532 eV, contrary to experimental evidence. Considering that at $h\nu$ = 650 eV the photoemission cross section is about 2.5 times larger for O1s than for C 1s electrons, we can safely conclude that the total amount of oxygen is only ~5 % of the G carbon atoms, while the additional peak at 284.3 eV corresponds approximatively to one-third of the G layer (see spectra IV).

The outcome of the analogous experiment performed on the S-contaminated sample (G^S experiment) is shown in Fig. 2. The bare Ni (111) surface was exposed to 1.7×10^{-5} mbar of C_2H_4 for 600 s at 823 K as described in Refs. [32,34]. However, due to a S contamination (see Fig. 2 right panel) originating from the rest vacuum, the G layer exhibits a mixture of G forms in agreement with previous reports [22,54]. The C 1s spectrum recorded immediately after growth (central panel, spectrum I) shows three main features at 283.2 eV, 283.8 eV and 284.3 eV, corresponding to Nickel carbide, dissolved carbon [54] and weakly interacting G [4,32,54], respectively. An additional component due to top-bridge graphene (284.7 eV) is also present. After exposure to C_2H_4 the sample is almost oxygen-free, as apparent from the O 1s spectrum I in the left panel.

Upon exposing the sample to 1 mbar of H_2 (spectra II and III) with traces of CO_2 and water (each of them <0.1 %), the C 1s and the O 1s spectra change; now, the O 1s region shows a feature at 529.3 eV, indicative of the formation of NiO, and a further moiety around 531 eV. The latter peak was attributed to OH by Salmeron et al. [12] and by Dedkov et al. [55], who also considered that it could be due to defects in the NiO patches. Therefore, it is reasonable that part of the Ni surface is not covered by graphene and gets hydroxylated, while the presence of carbonate on NiO is ruled out by the absence of a corresponding C1s signal around 289 eV.

The O 1s spectra II and III are quite similar to those observed after exposure of Ni(111) to CO_2 [12] in the mbar range, so that the formation of NiO is most likely caused by this gas. The peak at 531.2 eV is indeed explained by oxygen at defects according to Ref. [56]. For this reason even if H_2O is present in amount comparable with CO_2, we address the GS experiment as performed in H_2 and CO_2.

In the C 1s spectra, the centroid of the photoemitted lines shifts to higher BE. Spectrum II can be still described by including the same components used to fit the GC sample while spectrum III requires an additional component at 285.4 eV (thin red line in the central panel), that persists after pumping H_2 away (spectrum IV).

After recording spectrum IV, the sample was kept in vacuum for several hours at RT and was eventually annealed in H_2 pressure (with traces of CO_2 and H_2O). The resulting spectra are reported in Fig. 3.

Almost no changes occur in the O 1s and C 1s spectra until T~400 K (spectra I and II). Above this temperature, NiO (529.5 eV line) is promptly reduced (spectrum III) and disappears around 450 K (spectrum IV). In the corresponding C 1s spectra, the additional component at 285.4 eV converts gradually into a mixture of strongly and weakly interacting graphene. The system can be described with the same components used to describe the G^C experiment (285.3 eV and the three times larger component at 284.3 eV) only above T = 400 K.

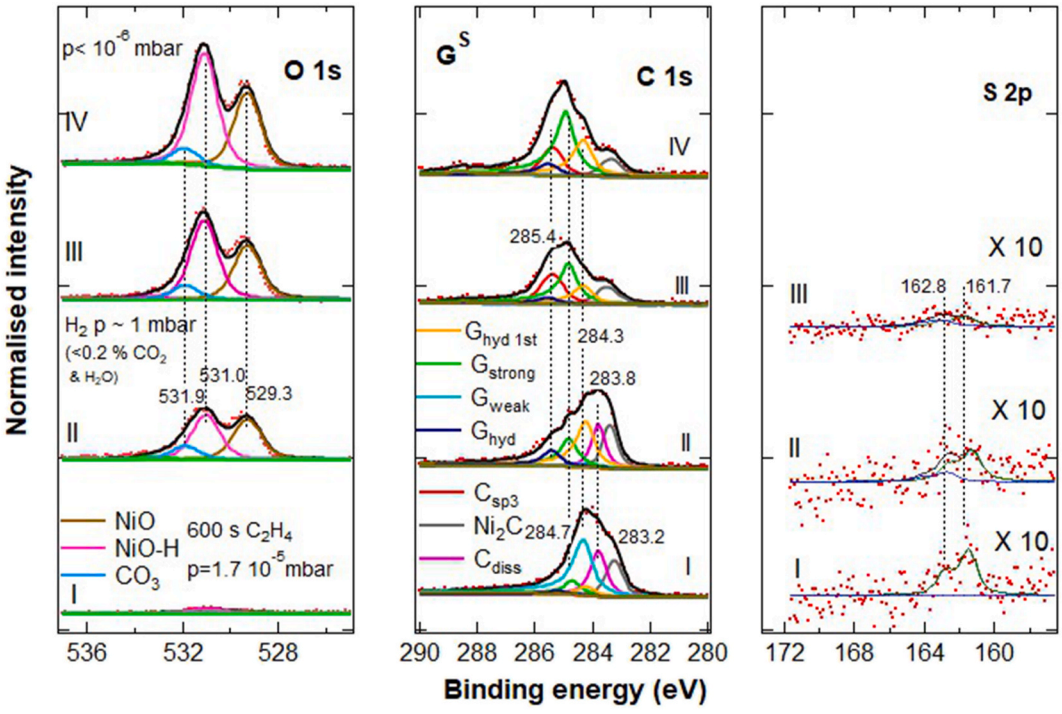

Fig. 2. G^S experiment at SLS: Transformation of G upon exposure to slightly contaminated H_2. XPS spectra of the O 1s (left), C 1s (center), and S 2p (right) regions recorded after G growth (spectrum I), during gas exposure (spectra II and III) and after evacuating the chamber (spectrum IV). Spectrum II started after 4 min exposure to H_2 and lasted ≈11 min. The sample was kept under H_2 for further 15 min and spectrum III was recorded eventually. 15 min later the chamber was evacuated, and spectrum IV was acquired. The data are shown in red while the black trace results from the fitting procedure. The data are normalized on the background at low BE for the different regions and upshifted for sake of clarity. Note the ten times magnification of the intensity of all S 2p spectra. (For interpretation of the references to color in this figure legend, the reader is referred to the Web version of this article.)

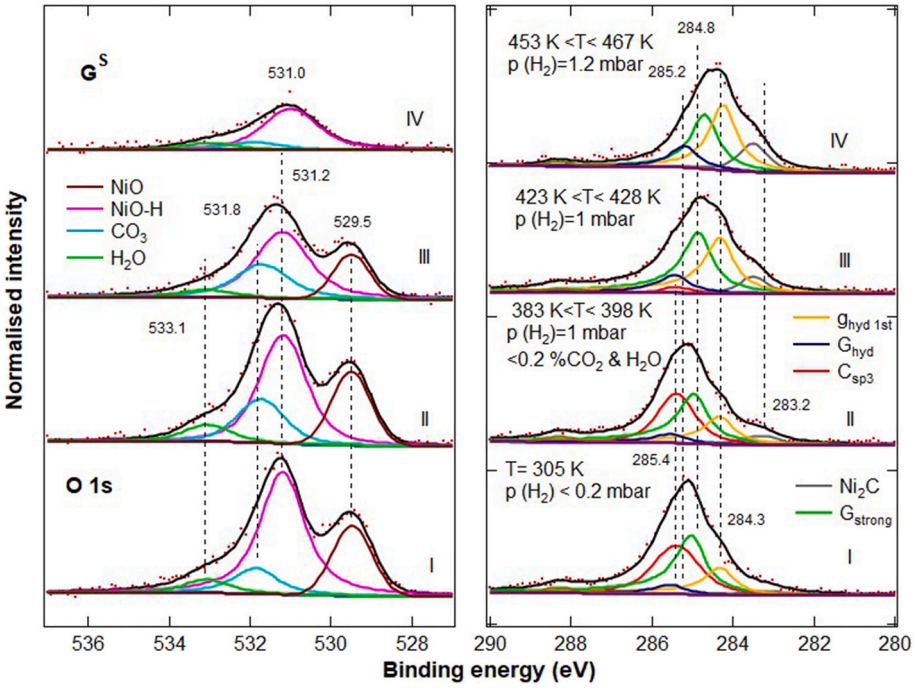

Fig. 3. G^S experiment: Reduction of NiO by H_2. XPS spectra (I-IV) are recorded under the same conditions as for the experiments of Fig. 2 for the O 1s (left) and C 1s (right) lines. Spectrum I was recorded after 6 min exposure while raising the pressure to 0.2 mbar; spectrum II started 12 min after the end of spectrum I; spectrum III started after further 12 min and spectrum IV after further 21 min. The initial and the final temperature while recording each spectrum is shown.

Further information can be obtained from the analysis of the Ni 2p region, which will be presented in the discussion section.

3.2. Theoretical results

To clarify the observed evolution of the C 1s spectra in both G^C and G^S experiments and to accurately assign the different C species identified during the fitting procedure, we performed DFT calculations on model systems representing the hydrogenated G/Ni interface.

In the G^C scenario, two types of carbon atoms, C fcc and C top, can undergo hydrogenation. Our calculations show that C fcc is energetically favored by ≈ 0.7 eV. When hydrogenated (Fig. 4a - $1H^{fcc}$/G/Ni), the C atom bonded to H undergoes pyramidalization, indicating a change in hybridization from sp^2 to sp^3. This explains why C fcc atoms are more prone to hydrogenation, since they exhibit weaker interaction with the underlying Ni atoms. Conversely, rehybridization of C top atoms is less favorable, as it would decrease their interaction with the metal.

When adding a second H atom ($2H^{fcc}$/G/Ni), we find no difference in energy whether the two atoms are close together or far apart, as long as they occupy the same sublattice (i.e. fcc). Then, we increased the

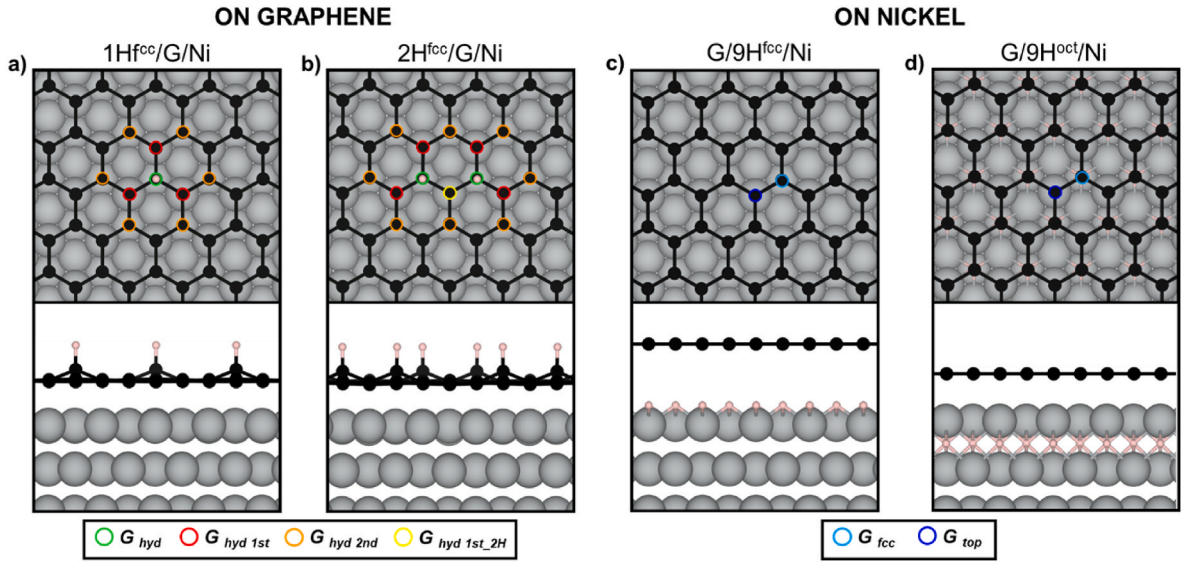

Fig. 4. Ball-and-stick model of DFT optimized structures (top and side view) of hydrogenated models of G/Ni. H adsorption on a-b) G, c) Ni, and d) interstitial octahedral sites within Ni. Non-equivalent C atoms, which are considered for the CLS values reported in Table 1, are highlighted with colored circles, as detailed in the legend below. Color coding: Ni atoms are rendered in grey; C atoms in black; H atoms in white. (For interpretation of the references to color in this figure legend, the reader is referred to the Web version of this article.)

coverage up to 9 H atoms, which corresponds to a full hydrogenation of the fcc sublattice given the size of our supercell model. In terms of energetics, the adsorption energies per H atom (ΔE_H, defined in the Computational Detail Section 2.2) are −0.04, −0.04, −0.03, and +0.16 eV for one, two, three, and nine H atoms, respectively. Considering the entropic cost associated with H_2 dissociation and adsorption, these results indicate that achieving high coverages is highly unlikely. Consequently, we expect that hydrogenation will primarily lead to the formation of isolated C–H bonds involving C atoms in the fcc position.

Based on these model structures, we computed the CLSs of the various carbon atoms, as shown in Table 1.

CLS values for hydrogenated systems are referenced to the carbon atoms of the G/Ni system (set as 0) in corresponding position (i.e. top or fcc).

The simulations show that at low H coverage ($1H^{fcc}$/G/Ni) the core level shift is positive (+0.49 eV) for the fcc C bound to H (C_{fcc}-H, highlighted in green in Fig. 4a, addressed as G_{hyd} in the following) while it is negative for the first neighbor C atom (C_{top}, highlighted in red in Fig. 4a, addressed as $G_{hyd\ 1st}$ in the following). The effect of hydrogenation appears to be predominantly local, as evidenced by the absence of change in the CLS value when considering the second neighbor C atom (C_{fcc}, highlighted in orange in Fig. 4a, referred to as $G_{hyd\ 2nd}$ hereafter).

As the hydrogen coverage increases, the core level shift of G_{hyd}, initially positive, decreases ($2H^{fcc}$/G/Ni in Fig. 4b), nearly vanishes for $3H^{fcc}$/Gr/Ni, and eventually turns negative at higher hydrogen coverage ($9H^{fcc}$/Gr/Ni).

The core-level shift of the neighboring non-hydrogenated C_{top} atom ($G_{hyd\ 1st}$) becomes slightly more negative while the core-level shift of the C_{top} atom between two hydrogenated C atoms ($G_{hyd\ 1st\_2H}$, highlighted in yellow in Fig. 4b, present only at higher coverage) becomes more and more negative as the H coverage increases.

Such theoretical predictions are in very good agreement with experimental findings obtained by using atomic H [27] and can thus be safely used for the assignment of the experimental spectra of the present experiment.

We also calculated the dissociation barrier for H_2 on free standing and Ni(111) supported G. As shown in Fig. 5, dissociation of H_2 on free standing G is largely endothermic (by +1.81 eV), with a dissociation barrier of 4.27 eV (blue line); vice versa, dissociation of H_2 on G/Ni(111) is slightly exothermic (−0.04 eV) and the barrier is reduced to 1.96 eV (red line).

Note that the lowest energy hydrogenation products differ between the free-standing and Ni(111)-supported cases. In the free-standing case, hydrogenation occurs on two adjacent C atoms from different C sublattices. In contrast, in the Ni(111)-supported case, hydrogenation involves two neighboring C atoms within the same fcc sublattice.

Table 1
Theoretically calculated core level shifts (ΔCLSs) with respect to strongly interacting G (G/Ni) for different H coverage on graphene (nH^{fcc}/Gr/Ni). CLS values for all systems have been calculated with respect to a non-interacting CH_4 molecule added to each system (as described in the Method section).

		ΔCLS (eV)
G/Ni	C_{top}	0
	C_{fcc}	0
$1H^{fcc}$/G/Ni	G_{hyd}	+0.49
	$G_{hyd\ 1st}$	−0.47
	$G_{hyd\ 2nd}$	−0.02
$2H^{fcc}$/G/Ni	G_{hyd}	+0.36
	$G_{hyd\ 1st}$	−0.53
	$G_{hyd\ 1st\_2H}$	−0.91
$3H^{fcc}$/G/Ni	G_{hyd}	+0.09
	$G_{hyd\ 1st}$	−0.57
	$G_{hyd\ 1st\_2H}$	−0.95
$9H^{fcc}$/G/Ni	G_{hyd}	−1.14
	$G_{hyd\ 1st\_3H}$	−1.97

4. Discussion

Following the outcome of the DFT calculations, we fitted the C 1s spectra of Fig. 1 with the Ni_2C (283.4 eV) and strongly interacting graphene (284.7 eV) components and with two additional contributions at 285.3 eV and 284.3 eV in 1:3 intensity ratio. These last components consider the presence of hydrogenated graphene in the low H coverage limit, according to the calculated CLS, and allow to obtain a good fit. We can therefore safely assign the peak at 285.3 eV to hydrogenated G at fcc sites (G_{hyd}) and the peak at 284.3 eV to graphene atoms in the 1st neighboring sites of hydrogenated C ($G_{hyd\ 1st}$). The area of the G_{hyd} peak is 0.06 of the total G area, indicating that 6 % of the C atoms in the G layer are hydrogenated and confirming the validity of our computational model.

The alternative assignment of the peak at 285.3 eV to intercalated CO is excluded because: i) CO should de-intercalate upon annealing to 353 K [52] while the intensity of the feature at 285.3 eV increases at least up to 457 K (Fig. 1); ii) the O 1s spectrum shows only a minor increase in intensity at the expected BE for bridge and on-top CO (531.0 eV and 532.2 eV [4,52]– see also Fig. S2 and relative discussion in the SI).

We can therefore safely conclude that the full monolayer G on Ni (111) is partly hydrogenated.

Based on XPS data, we cannot rule out either that some H ends subsurface, since this would not lead to a detectable change in the CLS, or that some H_2 intercalation occurs. This latter effect must be small but present. In fact, significant intercalation would cause some detachment of the G adlayer, corresponding to the appearance of a C 1s component with a negative CLS of around −0.7.eV (see Table 2 below), contrary to experimental evidence. On the other hand (Fig. S3), the normalized intensities of the components assigned to hydrogenated G and to its first neighbor increase after evacuation of the H_2/CO mixture at 457 K. This probably indicates that some H adsorbed on Ni(111) under G detaches from Ni and hydrogenates G. Therefore, our data suggest that intercalation of H_2 and dissociation at Ni sites is not the dominant path for H_2 molecules, although it must be present in small amount.

Upon annealing to 823 K (Fig. S3) the H coverage decreases, as previously reported in experiments where hydrogenation was performed with atomic H [27].

Pozzo et al. previously estimated the adsorption energy ΔE_H to be approximately −2.4 eV for a single H atom on G and approximately −2.1 eV for H on Ni(111) under G [57]. Such values are compatible with ours considering that our calculations are referenced to gas-phase H_2 (dissociation energy of 4.52 eV) and not to atomic H. Therefore, hydrogenation of G on the vacuum side is slightly exothermic while dissociation under G is slightly endothermic. Consequently, it is energetically possible for H_2 to intercalate, dissociate at the Ni(111) surface and then hydrogenate G. However, our study shows that, although present, this is not the main path for reacting H_2.

We demonstrate here that direct dissociation of H_2 at G is also possible.

The large reduction of the activation barrier for H_2 dissociation on G supported on Ni(111) (from 4.27 eV for freestanding G to 1.97 eV - see Fig. 5) indicates that the presence of the Ni substrate can significantly affect the reactivity of the graphene layer. Our NAP experiment in the mbar pressure range is in the middle of the gap between UHV studies (for which no hydrogenation was observed after several thousands Langmuir of H_2 exposure [58] and high-pressure studies (some hydrogenation was observed for exfoliated G upon exposure at a pressure of 24 bar [28]). Coherently, the value of the reduced barrier (1.97 eV) is high enough to explain previous experimental results both in UHV and in catalytic conditions. However, an even lower barrier for H_2 dissociation of the order of ≈1 eV would be necessary to account for the attained coverage on a perfect G/Ni(111) layer. This discrepancy is easily justified considering that in a real experiments supported G is not exactly flat (as in DFT simulations) but can present bended areas (e.g. above steps on the substrate), edges of domains and point defects where

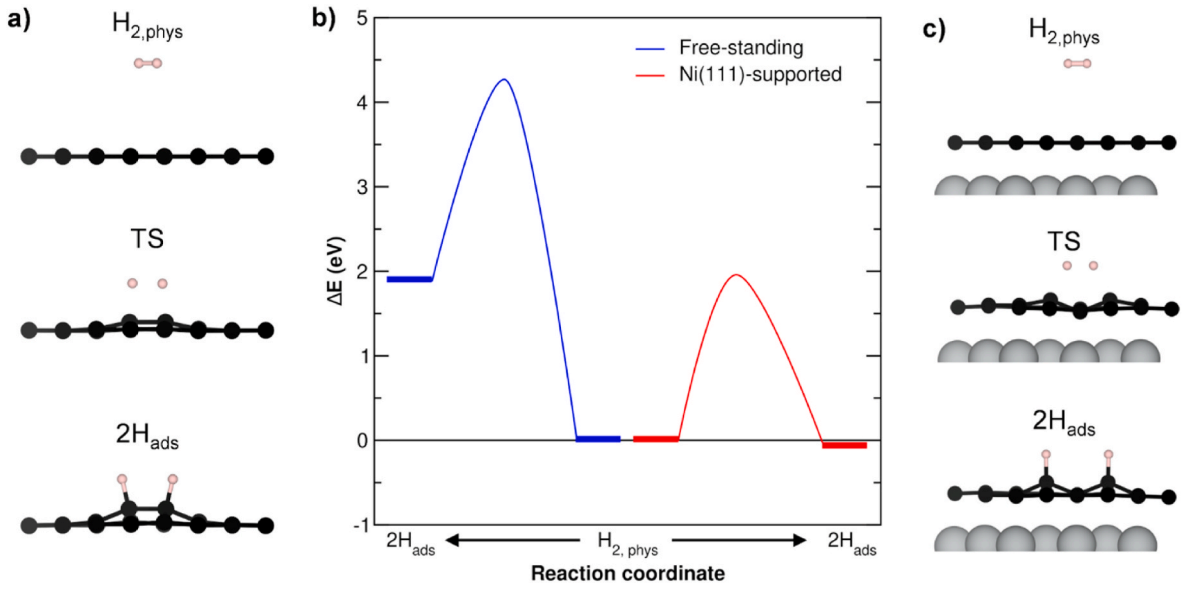

Fig. 5. Side views: Configurations for the initial state ($H_{2,\ phys}$), the transition state (TS), and final state (2 H_{ads}) configurations for H_2 dissociation on top of (a) free-standing G and (c) G/Ni(111). (right). The corresponding energy profile of the three states (as obtained through a CI-NEB calculation) for H_2 dissociation is reported in panel (b). The free-standing graphene and Ni(111)-supported graphene cases are shown in blue and red, respectively. Color coding: Ni atoms in grey, C atoms in black, H atoms in white. (For interpretation of the references to color in this figure legend, the reader is referred to the Web version of this article.)

Table 2
Theoretically calculated core level shifts for G on hydrogenated Ni (ΔCLSs) with respect to the strongly interacting G (G/Ni) system for different H coverage on graphene (Gr/nH/Ni). CLS values for all systems have been calculated with respect to a non-interacting CH_4 molecule added to each system (as described in the Method section). The two values reported for each configuration refer to the C atom in the fcc and top positions, respectively.

		ΔCLS (eV)
	G/Ni	0/0
Fcc	**G/2H/Ni**	−0.73/-0.59
	G/3H/Ni	−0.75/-0.61
	G/9H/Ni	−0.76/-0.65
Int	**G/2H/Ni**	−0.02/-0.01
	G/3H/Ni	−0.02/-0.07
	G/9H/Ni	−0.14/-0.14

the dissociation barrier can be lower than 1.97 eV. Moreover, the larger H coverage attained at the same H_2 pressure for the GS experiment (see the following - presenting NiO patches and different kinds of G, hence having an overall higher defectivity) and the fact that graphene grown by CVD is more effectively hydrogenated than exfoliated one [28] are well explained in this frame.

Alternatively, the dissociation barrier can be significantly lower for vibrationally excited molecules [59]: in our conditions we can estimate that at 457 K the probability to have vibrationally excited H_2 molecules in the $\upsilon = 1$ state is of the order of $\approx 10^{-6}$ so that at a pressure of 1 mbar each atom is hit every second by one vibrationally excited molecule.

In the presence of S contamination and, hence, of an incomplete and defective G layer (Fig. 2), the situation is more complex. The layer consists now of different C species, reasonably arranged in relatively small domains. The C 1s spectra of Fig. 2 can be fitted neither with the same fitting parameters used for the G^C sample nor with components corresponding to the predicted CLS for higher hydrogen coverage (see Table 1). Therefore, the additional component at 285.4 eV (red component in Figs. 2 and 3) cannot be assigned to hydrogenated *non-defective* G.

On nano porous graphene [60], a contribution at around 285.3 eV in the C 1s spectrum becomes prominent after exposure to atomic deuterium, and it is assigned to sp^3-like distorted bonds. C 1s maps show an increase in the high energy tail (and thus an increased sp^3 intensity) close to pores [61]. Our spectra could therefore indicate the presence of hydrogenated C atoms at G defects. Such an assignment would also agree with previous experiments on carbon nanotubes, for which hydrogenation leads to the appearance of a broad contribution between 285 and 286 eV in the C 1s region [62].

As possible alternative assignments, we considered the formation of.

a) Top-hcp graphene domains on hydrogenated Ni atoms;
b) Graphone or graphane;
c) Isolated CH_x species;
d) CO, methoxy or other O containing species;

However, all these hypotheses are discarded since.

a) We performed DFT calculations to investigate the hydrogenation of both surface and subsurface Ni. Starting with the top-fcc registry and gradually increasing the coverage up to 9 H atoms, we identified the preferential adsorption sites to be the fcc hollow for hydrogenation on top of Ni and the octahedral interstitial sites for hydrogenation in the Ni subsurface region. In the former case (Fig. 4c), G decouples from Ni due to the intercalated H atoms, while in the latter case (Fig. 4d), the G-Ni vertical distance remains unchanged. This difference in the geometrical structure reflects a change in the interaction between G and Ni. Indeed, when H chemisorbs on the Ni surface, it becomes negatively charged, taking electron charge density from the Ni (see Fig. S4a). Consequently, this results in the lifting of the graphene layer (from 2.1 Å to 3.7 Å), shifting its doping level from n-doped (G/Ni) to neutral (G/nH/Ni). As a result of this decoupling, carbon (C) atoms of the graphene layer situated above the hydrogenated Ni experience a negative core-level shift (CLS) compared to G/Ni (Table 2), which is incompatible with the experimental binding energy (BE) of 285.4 eV, corresponding to a positive core-level shift.

When hydrogen occupies octahedral sites in the Ni subsurface layer, the interaction between G and Ni remains almost unaffected (as evidenced by the unchanged atomic charge on G in Fig. S4b). As a result, the core-level shift (CLS) values do not change compared to the pristine case (as shown in Table 2). Therefore, this possibility

must also be excluded. We also considered that hydrogenation may change the G-Ni registry from top-fcc to top-hcp. However, the situation remains unchanged both qualitatively and quantitatively, with the CLSs being in perfect line with the values computed for the top-fcc system.

b) At variance with the outcome of our experiment, graphone has a C 1s peak at 284.3 eV [63] and graphane has two C 1s peaks of comparable intensity at 284.7 eV and 285.3 eV [27,64].

c) The peak at 285.4 eV cannot be assigned to isolated CH_x species since they were identified with peaks at lower BE (~285.0 eV for CH_x and 284.3 eV to CH) by Degerman et al. [65]. Moreover, these species were produced at a ~100 times higher pressure than in the present experiment, i.e. under conditions for which methanation is definitely more likely to occur. Finally, Ceyer and coworkers [66] demonstrated that CH_3 dissociates on Ni(111) below room temperature in UHV, leading to CH formation. On the contrary, the species with BE 285.2–285.4 eV persists after evacuating the chamber (spectrum IV in Fig. 2, central panel) and even increases while remaining in vacuum (spectrum I in Fig. 3) with the sample at RT.

d) Finally, the peak at 285.4 eV cannot be ascribed to CO or other oxygen containing species such as methoxy or graphene oxide, since its increase is not correlated to any O 1s component (see Fig. 2 and left panel of Fig. S5 in SI). Indeed, CO at bridge or multi-coordinate positions [12] is characterized by an O1s component around 531 eV, while on-top CO presents an O 1s line at 532 eV. If the 285.4 eV peak were related to this last species, the 532 eV intensity would be expected to be much larger, considering the cross sections for O 1s and C 1s photoemission at $h\nu = 742$ eV. Indeed, the O 1s spectrum is almost unaffected by the formation of the 285.4 eV moiety, except for the appearance of minor peaks at 531.9 eV and 533 eV (see spectrum IV in Fig. 3), that we assign to traces of carbonates [67] and water, respectively. The alternative possible assignment of the peak at 531.9 eV to CO at on-top sites (with a partner C 1s line at 285.8 eV, that could be present in the tail of the main C 1s line) is less convincing since CO adsorption on Ni is expected to be poisoned by the S-contamination (see right panel of Fig. 2).

H at G defects would not show up in our DFT simulations based on a well-ordered single layer of G, while the surface in the GS experiment has coexisting G and Ni oxide/hydroxide patches and presents, at least initially, a S contamination.

We further note that.

1) since the dominant peak in spectrum IV of Fig. 2 is above 285 eV, oxidized Ni is *not* covered by G; the C 1s BE of G on NiO should be indeed the one of weakly interacting G [55], contrary to experimental evidence;
2) strongly interacting G/Ni(111) coexists with the 285.2–285.4 eV moiety.

We can thus conclude that, during exposure to H_2 (spectra II and III), our surface consists of patches of strongly interacting graphene and of Ni oxide and/or hydroxide. Our tentative picture is that the G edges close to NiO are easily hydrogenated and give rise to the sp^3 peak. The decrease of the 285.4 eV species when NiO starts to be reduced (Fig. 3) supports this explanation.

Finally, we assign the peak at 533 eV to water contamination. The alternative assignment to physisorbed CO_2 under the G sheet is excluded since no companion feature at 291 eV is present (see Fig. 2) and since the peak persists upon evacuation of the experimental chamber with the sample at room temperature (RT), at variance with the behavior previously observed in Refs. [4,32].

Inspection of the S 2p region shows that initially (Fig. 2, spectrum I) some Ni sulfide (BE at 161.2 eV and 162.8 eV [68]) is present. When graphene starts to form, a second, weaker doublet appears at higher BE (blue line in the same panel), compatible with the one reported for S doped G (S $2p_{3/2}$ line at 163.9 eV [69]). Therefore, we assign it to traces of S bound to C, indicating a slight S-doping of the graphene layer.

The presence of S favors the formation of less strongly interacting G (see spectrum I in Fig. 2) with respect to strongly interacting one, in qualitative agreement with recent findings that indicate a weakening of graphene-substrate interaction in presence of S [22].

We believe, however, that the higher H coverage attained starting with the initially S contaminated sample is due to the presence of NiO and not directly to sulfur for the following reasons.

a) as apparent from Fig. 2 when the amount of sp^3 is largest (spectrum III) sulfur has already decreased due to interaction with H_2;
b) NiO has a larger lattice spacing than Ni(111) [70] so that coexisting G patches are expected to be corrugated and thus more conducive to H_2 dissociation [71] than unstrained G.

To gain a more quantitative understanding of the experiment, we report in Fig. 6 the coverage of the different components while annealing the GS sample in H_2. To allow for a straightforward comparison of the data, the areas obtained by the fits were corrected for the different attenuation of the C 1s and O 1s intensities at $h\nu = 742$ eV (see Fig. S1) and divided by the expected excitation cross section [72]. This analysis indicates that the total amount of carbon initially present at the surface is about twice the total amount of oxygen.

The transmission function of the photoelectron analyzer is close to constant in the measured kinetic energy range, with a possible error of at most ±20 % between the C 1s and O 1s signals.

An absolute calibration of the coverage as done in Ref. [32] is not feasible in the present case since G is not likely to cover the whole surface.

Analysis of the O 1s components (left panel of Fig. 6) indicates that both *NiO and carbonates* disappear around 423 K. OH decreases in the same temperature range, but it does not vanish. This observation is in line with the one of Salmeron and coworkers [12], who studied the reduction of NiO on bare Ni(111) by CO_2 under NAP conditions.

The right panel in Fig. 6 reports the thermal evolution of the C 1s components. It shows that the disappearance of the sp^3 carbon is clearly correlated with the removal of the NiO and with the reduction of NiOH patches. This leaves space for the growth of G and carbide. Hydrogenation of these new G areas contributes to the increase of G_{hyd}. The 20 % decrease of the total C intensity at high T can be due, at least partially, to the slight increase of carbide, which has a lower carbon density than graphene; however, it is reasonable that such a decrease is overestimated, since the coverage is obtained from the areas without correcting for the change in the position of the sample or the flux.

The fraction of the surface covered by G and by oxidized/hydroxilated Ni can be estimated from the analysis of the Ni 2p line recorded before and after reduction with H_2 (see Fig. 7). We fitted the spectra by using the three major components both for Ni and for NiO, as reported in Ref. [73], and fixing the BE and the spin-orbit split according to literature values. Table 3 shows the resulting areas (normalized to the background at the low BE side of the spectra) for the different components before and after reduction.

In principle, also contributions from Ni hydroxide could be present. However, the main lines of $Ni(OH)_2$, NiOOH and NiO are very close in BE (at BE = 855.3 eV, 855.8 eV and 854.7 eV, respectively [74]) and hardly resolvable in our spectra. Therefore, we consider that the NiO envelope is representative of both Ni oxide and hydroxide species. The validity of this approximation is supported by the results reported by Marcus et al. [70], who exposed a NiO/Ni(111) film at 300 K to 150 L of water vapor. Almost no change in the Ni 2p spectrum is observed after exposure, despite an evident increase of the OH-related line at BE = 531.4 eV in the O 1s region.

In the present experiment, 75 % of the probed Ni atoms are in the form of Ni oxide/hydroxide before reduction, while such percentage reduces to 21 % after reduction. Inspection of the O 1s spectrum

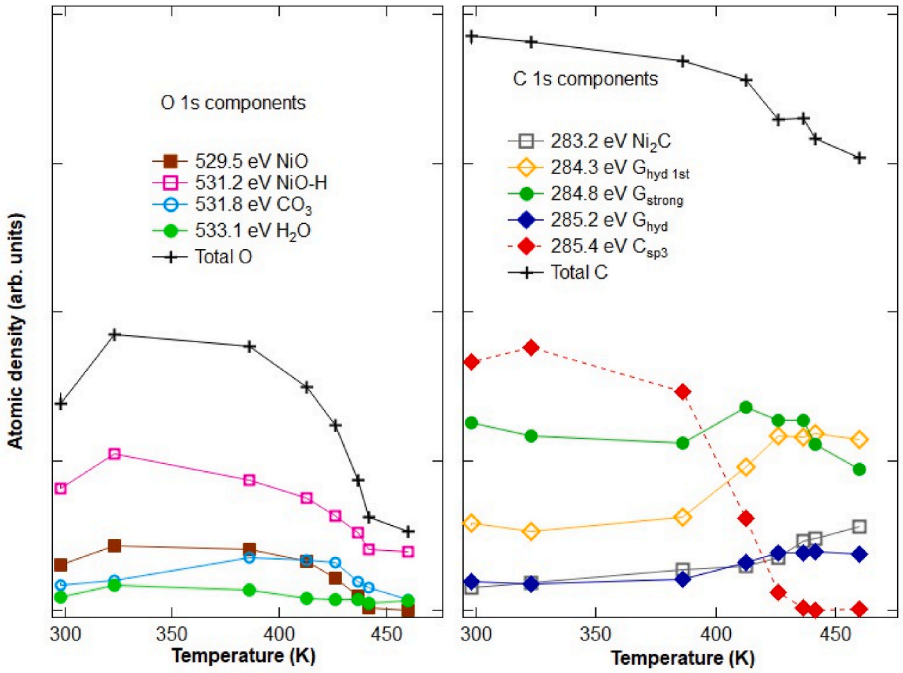

Fig. 6. Temperature dependence of the coverage during the reduction of the GS sample. Left panel: O 1s components; right panel: C 1s components. The coverage is reported in arbitrary units since a reliable absolute calibration is not feasible (see text).

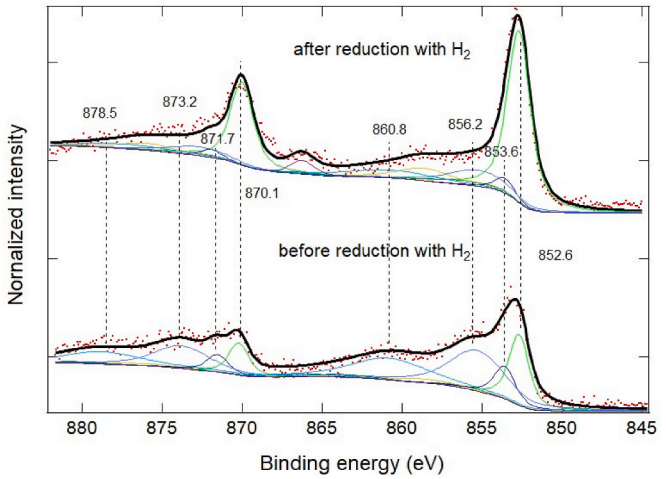

Fig. 7. Ni 2p line before (lower spectrum) and after (upper spectrum) reduction. Spectra are recorded with hν = 1065 eV. The green line indicates the metallic contribution while the three blue ones indicate the NiO components according to Ref. [73]. The data are normalized on the low BE side of the spectrum. An additional peak at 866.3 eV was necessary to properly fit the spectrum after reduction. Its assignment is not obvious but its intensity amounts to only 2 % of the total Ni 2p intensity and thus does not affect our conclusions. (For interpretation of the references to color in this figure legend, the reader is referred to the Web version of this article.)

indicates that about 40 % of this amount is due to NiO and the remaining 60 % is due to hydroxylated Ni. Furthermore, the former spectrum looks intermediate between those reported in literature for 0.7 ML and 1.5 ML NiO thin films grown on Ag(100) [75], indicating that NiO covers a significant fraction of the surface. However, it was demonstrated that during oxidation of Ni(111) fast nucleation with lateral growth of 2 ML thick NiO patches occurs [76], so that we expect that initially less than 75 % of the surface is covered by Ni oxide/hydroxide.

On the other hand, from Fig. 6 the estimated C/O ratio is 2.3 before reduction. The actual amount of carbon can be obtained by comparing the C 1s intensity in the GS and GC experiments. For the GC experiment, it is possible to estimate that G covers ≈80 % of the surface and Ni_2C covers 20 % [4], corresponding to a G coverage of the order of ≈1.6 ML (in ML of Ni(111)). Scaling the corresponding normalized intensity and correcting for the different cross sections in the G^C and G^S experiment (which is 1.5 times larger at 650 eV than at 742 eV [72]), we estimate the C coverage to be ~ 0.8 ML (spectrum I in Fig. 2) after C_2H_4 exposure and to increase to 1.14 ML (spectrum I in Fig. 3) before reduction with H_2. As apparent from Fig. 6, before reduction ≈0.04 ML of C is in the form of Ni_2C while the remaining ≈1.1 ML is in the form of clean or hydrogenated G or of sp^3-hybridized C. Recalling that in the Ni_2C patches there is one C atom every two Ni atoms while in graphene the ratio is 2:1, it is reasonable to conclude that Ni_2C covers at most 8 % of the surface and that ~55 % of the surface is covered by G in its different forms. The remaining 37 % of the surface consists of Ni oxide/hydroxide. Considering the experimental errors in the fitting procedure, this coverage is compatible both with the C/O ratio estimated in Fig. 6 and

Table 3
Areas of metallic Ni components and oxidized Ni components as resulting from the fitting of Fig. 7. The lower total intensity of the Ni 2p before reduction most likely arises from changes in the position of the sample.

	Binding energy (eV)	Normalized intensity before reduction	Normalized intensity after reduction
Metallic Ni	852.7	$2.35 \cdot 10^5$	$9.93 \cdot 10^5$
	856.2	$0.17 \cdot 10^5$	$7.20 \cdot 10^5$
	858.6	$0.45 \cdot 10^5$	$1.87 \cdot 10^5$
Oxidized Ni	853.6	$1.26 \cdot 10^5$	$0.77 \cdot 10^5$
	855.3	$3.97 \cdot 10^5$	$2.41 \cdot 10^5$
	860.8	$3.06 \cdot 10^5$	$1.85 \cdot 10^5$
	866.4	$0.35 \cdot 10^5$	$0.19 \cdot 10^5$
	864.1	$0.31 \cdot 10^5$	$0.18 \cdot 10^5$
	866.3	0	$0.52 \cdot 10^5$
Total metallic Ni		$2.97 \cdot 10^5$	$19.77 \cdot 10^5$
Total NiO		$8.95 \cdot 10^5$	$5.4 \cdot 10^5$
NiO fraction		0.75	0.21

with the information derived from Ni 2p spectra that 75 % of the probed Ni atoms are in the form of Ni oxide/hydroxide, admitting that most of it is organized in bilayer islands.

By comparing the area of the S 2p and of the C 1s peaks, it is also possible to estimate the initial coverage of S, which is about 4 % of the C coverage present at the surface.

5. Conclusions

We have investigated the hydrogenation of G following exposure to methanation mixtures (CO or $CO_2 + H_2O$ in large excess of H_2) at a total pressure of 1 mbar by Near Ambient Pressure XPS.

The different components of the C1s line have been assigned by using core-level shifts obtained with ab-initio methods for hydrogenated graphene.

For a full and non-defective G monolayer, a relatively low H coverage is attained, in good agreement with previous results obtained using atomic H [27] and with our DFT calculations. The presence of the Ni substrate makes H_2 dissociation at G slightly exothermic and reduces the H_2 dissociation barrier to 1.97 eV. Further reduction is probable for G carbon atoms at bent sites on Ni steps.

In the presence of sulfur contamination, on the contrary, the C layer consists of a mixture of nickel carbide, dissolved carbon and weakly interacting G. Exposing such a surface to H_2 with traces of CO_2 an incomplete G layer mixed with NiO–NiO–H patches is obtained.

The attained H coverage is then significantly larger than for a full, non-defective G monolayer, as indicated by the presence of a strong sp^3 component around 285.4 eV in the C 1s spectrum. The higher H coverage on G attained in the presence of NiO patches can be explained by the lower adsorption energy of H at Ni–NiO interfaces, which makes adsorption at G energetically viable [77], and/or by the higher defectivity of the G layer, which might further reduce the activation barrier for H_2 dissociation.

CRediT authorship contribution statement

Giovanni Carraro: Writing – review & editing, Software, Methodology, Investigation. **Sina Ebrahim Atakoohi:** Writing – review & editing, Investigation. **Daniele Perilli:** Writing – review & editing, Writing – original draft, Software, Methodology, Investigation. **Ola Alayan:** Writing – review & editing, Data curation. **Gianangelo Bracco:** Writing – review & editing, Methodology. **Gabriella Garbarino:** Writing – review & editing, Methodology, Investigation, Funding acquisition. **Paul M. Leidinger:** Writing – review & editing, Methodology. **Zbynek Novotny:** Writing – review & editing, Methodology. **Mario Rocca:** Writing – review & editing, Writing – original draft, Methodology, Funding acquisition. **Letizia Savio:** Writing – review & editing, Writing – original draft, Methodology, Investigation, Funding acquisition. **Marco Smerieri:** Writing – review & editing, Software, Methodology, Investigation. **Cristiana Di Valentin:** Writing – review & editing, Software, Investigation, Funding acquisition. **Luca Vattuone:** Writing – original draft, Supervision, Investigation, Funding acquisition, Formal analysis, Conceptualization.

Declaration of competing interest

The authors declare the following financial interests/personal relationships which may be considered as potential competing interests: Luca Vattuone reports financial support was provided by MIUR. Cristiana Di Valentin reports financial support was provided by MIUR. Mario Rocca reports was provided by MIUR. Letizia Savio reports financial support was provided by MIUR. Luca Vattuone reports equipment, drugs, or supplies was provided by SOLEIL. Luca Vattuone reports equipment, drugs, or supplies was provided by Paul Scherrer Institute PSI. Associate Editor Cristiana Di Valentin. If there are other authors, they declare that they have no known competing financial interests or personal relationships that could have appeared to influence the work reported in this paper.

Acknowledgment

D.P. and C.D.V. acknowledge funding from the European Union – NextGenerationEU through the Italian Ministry of University and Research under PNRR – M4C2I1.4 ICSC – Centro Nazionale di Ricerca in High Performance Computing, Big Data and Quantum Computing (Grant No. CN00000013 and Innovation Grant with Leonardo and Ferrovie dello Stato).

L.S. and M.R. acknowledge funding from the European Union – NextGenerationEU through the Italian Ministry of University and Research under projects PRIN2022 2022LS74H2 and PRIN-PNRR P20227XSAH.

L.V. acknowledge funding from Ministry of University and Research under projects PRIN2017 KF MJ8E_003.

G.G. acknowledges the Project funded under the National Recovery and Resilience Plan (NRRP), Mission 4 Component 2 Investment 1.3 - Call for tender No. 1561 of October 11, 2022 of Ministero dell'Università e della Ricerca (MUR); funded by the European Union – NextGenerationEU, PE0000021, "Network 4 Energy Sustainable Transition – NEST".

Part of this work was performed at the In Situ Spectroscopy (X07DB) beamline of the Swiss Light Source, Paul Scherrer Institut, Villigen PSI, Switzerland. We acknowledge the PSI for beamtime allocation and support.

Part of this work was done at the Tempo Beamline of Soleil Synchrotron Light Source. We acknowledge Soleil for beamtime allocation and support. We acknowledge in particular Dr. Rocco Davì as well as prof. Jean Jacques Gallet and prof. Fabrice Bournel for support during the measurements at Soleil.

We thank Andrea Fregara and Matteo Antonio Lucaccini (IMEM-CNR) for technical support.

Appendix A. Supplementary data

Supplementary data to this article can be found online at https://doi.org/10.1016/j.mtchem.2024.102359.

Data availability

Data will be made available on request.

References

[1] A. Dahal, M. Batzill, Graphene–nickel interfaces: a review, Nanoscale 6 (2014) 2548, https://doi.org/10.1039/c3nr05279f.

[2] G. Cui, Z. Bi, R. Zhang, J. Liu, X. Yu, Z. Li, A comprehensive review on graphene-based anti-corrosive coatings, Chem. Eng. J. 373 (2019) 104–121, https://doi.org/10.1016/j.cej.2019.05.034.

[3] Q. Fu, X. Bao, Surface chemistry and catalysis confined under two-dimensional materials, Chem. Soc. Rev. 46 (2017) 1842–1874, https://doi.org/10.1039/C6CS00424E.

[4] R. Davì, G. Carraro, M. Stojkovska, M. Smerieri, L. Savio, M. Lewandowski, J.-J. Gallet, F. Bournel, M. Rocca, L. Vattuone, Boudouard reaction under graphene cover on Ni(1 1 1), Appl. Surf. Sci. 599 (2022) 154065, https://doi.org/10.1016/j.apsusc.2022.154065.

[5] D. Prasai, J.C. Tuberquia, R.R. Harl, G.K. Jennings, K.I. Bolotin, Graphene: corrosion-inhibiting coating, ACS Nano 6 (2012) 1102–1108, https://doi.org/10.1021/nn203507y.

[6] T.-Y. Sun, Y. Hao, C.-T. Lin, L. Wang, L.-F. Huang, Unraveling the strong coupling between graphene/nickel interface and atmospheric adsorbates for versatile realistic applications, Carbon Trends 2 (2021) 100013, https://doi.org/10.1016/j.cartre.2020.100013.

[7] Y. Yao, Q. Fu, Y.Y. Zhang, X. Weng, H. Li, M. Chen, L. Jin, A. Dong, R. Mu, P. Jiang, L. Liu, H. Bluhm, Z. Liu, S.B. Zhang, X. Bao, Graphene cover-promoted metal-catalyzed reactions, Proc. Natl. Acad. Sci. USA 111 (2014) 17023–17028, https://doi.org/10.1073/pnas.1416368111.

[8] D. Perilli, S. Fiori, M. Panighel, H. Liu, C. Cepek, M. Peressi, G. Comelli, C. Africh, C. Di Valentin, Mechanism of CO intercalation through the graphene/Ni(111)

interface and effect of doping, J. Phys. Chem. Lett. 11 (2020) 8887–8892, https://doi.org/10.1021/acs.jpclett.0c02447.
[9] S. Del Puppo, V. Carnevali, D. Perilli, F. Zarabara, A.L. Rizzini, G. Fornasier, E. Zupanič, S. Fiori, L.L. Patera, M. Panighel, S. Bhardwaj, Z. Zou, G. Comelli, C. Africh, C. Cepek, C. Di Valentin, M. Peressi, Tuning graphene doping by carbon monoxide intercalation at the Ni(111) interface, Carbon N Y 176 (2021) 253–261, https://doi.org/10.1016/j.carbon.2021.01.120.
[10] S. Rönsch, J. Schneider, S. Matthischke, M. Schlüter, M. Götz, J. Lefebvre, P. Prabhakaran, S. Bajohr, Review on methanation – from fundamentals to current projects, Fuel 166 (2016) 276–296, https://doi.org/10.1016/j.fuel.2015.10.111.
[11] E. Vesselli, L. De Rogatis, X. Ding, A. Baraldi, L. Savio, L. Vattuone, M. Rocca, P. Fornasiero, M. Peressi, A. Baldereschi, R. Rosei, G. Comelli, Carbon dioxide hydrogenation on Ni(110), J. Am. Chem. Soc. 130 (2008) 11417–11422, https://doi.org/10.1021/ja802554g.
[12] C. Heine, B.A.J. Lechner, H. Bluhm, M. Salmeron, Recycling of CO_2 : probing the chemical state of the Ni(111) surface during the methanation reaction with ambient-pressure X-ray photoelectron spectroscopy, J. Am. Chem. Soc. 138 (2016) 13246–13252, https://doi.org/10.1021/jacs.6b06939.
[13] W. Erley, Sulfur poisoning of carbon monoxide adsorption on Ni(111), J. Catal. 53 (1978) 287–294, https://doi.org/10.1016/0021-9517(78)90101-X.
[14] M. Kiskinova, D.W. Goodman, Modification of chemisorption properties by electronegative adatoms: H2 and CO on chlorided, sulfided, and phosphided Ni (100), Surf. Sci. 108 (1981) 64–76, https://doi.org/10.1016/0039-6028(81)90358-7.
[15] K. Stangeland, D. Kalai, H. Li, Z. Yu, CO 2 methanation: the effect of catalysts and reaction conditions, Energy Proc. 105 (2017) 2022–2027, https://doi.org/10.1016/j.egypro.2017.03.577.
[16] B. Miao, S.S.K. Ma, X. Wang, H. Su, S.H. Chan, Catalysis mechanisms of CO_2 and CO methanation, Catal. Sci. Technol. 6 (2016) 4048–4058, https://doi.org/10.1039/C6CY00478D.
[17] A.S. Calbry-Muzky, T.J. Schildhauer, Direct methanation of biogas—technical challenges and recent progress, Front. Energy Res. 8 (2020), https://doi.org/10.3389/fenrg.2020.570887.
[18] P. Strucks, L. Failing, S. Kaluza, A short review on Ni-catalyzed methanation of CO2: reaction mechanism, catalyst deactivation, dynamic operation, Chem. Ing. Tech. 93 (2021) 1526–1536, https://doi.org/10.1002/cite.202100049.
[19] W.T. Owens, N.M. Rodriguez, R.T.K. Baker, Effect of sulfur on the interaction of nickel with ethylene, Catal. Today 21 (1994) 3–22, https://doi.org/10.1016/0920-5861(94)80030-8.
[20] K. Sagisaka, J. Nara, J.K. Wenderott, R. Kadowaki, A. Maruta, T. Abukawa, D. Fujita, Strong suppression of graphene growth by sulfur superstructure on a nickel substrate, Phys. Rev. Mater. 6 (2022), https://doi.org/10.1103/PhysRevMaterials.6.034007.
[21] R. Kikowatz, K. Flad, G. Horz, Effects of carbon and sulfur on the decomposition of hydrocarbons on nickel, J. Vac. Sci. Technol.: Vacuum, Surfaces and Films 5 (1987) 1009–1014, https://doi.org/10.1116/1.574174.
[22] B. Orbán, T. Höltzl, The promoter role of sulfur in carbon nanotube growth, Dalton Trans. 51 (2022) 9256–9264, https://doi.org/10.1039/D2DT00355D.
[23] H. Guo, J. Gao, N. Ishida, K. Sagisaka, D. Fujita, Growth of quadrilateral graphene flakes with a sulfur atomic template on the surface of Ni (110), Carbon N Y 153 (2019) 116–119, https://doi.org/10.1016/j.carbon.2019.06.102.
[24] M. Sarno, C. Cirillo, R. Piscitelli, P. Ciambelli, A study of the key parameters, including the crucial role of H2 for uniform graphene growth on Ni foil, J. Mol. Catal. Chem. 366 (2013) 303–314, https://doi.org/10.1016/j.molcata.2012.10.009.
[25] M.R. Habib, T. Liang, X. Yu, X. Pi, Y. Liu, M. Xu, A review of theoretical study of graphene chemical vapor deposition synthesis on metals: nucleation, growth, and the role of hydrogen and oxygen, Rep. Prog. Phys. 81 (2018) 036501, https://doi.org/10.1088/1361-6633/aa9bbf.
[26] K. Li, C. He, M. Jiao, Y. Wang, Z. Wu, A first-principles study on the role of hydrogen in early stage of graphene growth during the CH4 dissociation on Cu (111) and Ni(111) surfaces, Carbon N Y 74 (2014) 255–265, https://doi.org/10.1016/j.carbon.2014.03.030.
[27] M.L. Ng, R. Balog, L. Hornekær, A.B. Preobrajenski, N.A. Vinogradov, N. Mårtensson, K. Schulte, Controlling hydrogenation of graphene on transition metals, J. Phys. Chem. C 114 (2010) 18559–18565, https://doi.org/10.1021/jp106361y.
[28] B.H. Kim, S.J. Hong, S.J. Baek, H.Y. Jeong, N. Park, M. Lee, S.W. Lee, M. Park, S. W. Chu, H.S. Shin, J. Lim, J.C. Lee, Y. Jun, Y.W. Park, N-type graphene induced by dissociative H2 adsorption at room temperature, Sci. Rep. 2 (2012) 690, https://doi.org/10.1038/srep00690.
[29] D. Smith, R.T. Howie, I.F. Crowe, C.L. Simionescu, C. Muryn, V. Vishnyakov, K. S. Novoselov, Y.-J. Kim, M.P. Halsall, E. Gregoryanz, J.E. Proctor, Hydrogenation of graphene by reaction at high pressure and high temperature, ACS Nano 9 (2015) 8279–8283, https://doi.org/10.1021/acsnano.5b02712.
[30] L. Kyhl, R. Bisson, R. Balog, M.N. Groves, E.L. Kolsbjerg, A.M. Cassidy, J. H. Jørgensen, S. Halkjær, J.A. Miwa, A. Grubišić Čabo, T. Angot, P. Hofmann, M. A. Arman, S. Urpelainen, P. Lacovig, L. Bignardi, H. Bluhm, J. Knudsen, B. Hammer, L. Hornekaer, Exciting H_2 molecules for graphene functionalization, ACS Nano 12 (2018) 513–520, https://doi.org/10.1021/acsnano.7b07079.
[31] H. Liu, A. Zakhtser, A. Naitabdi, F. Rochet, F. Bournel, C. Salzemann, C. Petit, J.-J. Gallet, W. Jie, Operando near-ambient pressure X-ray photoelectron spectroscopy study of the CO oxidation reaction on the oxide/metal model catalyst ZnO/Pt(111), ACS Catal. 9 (2019) 10212–10225, https://doi.org/10.1021/acscatal.9b02883.
[32] R. Davì, G. Carraro, M. Stojkovska, M. Smerieri, L. Savio, M. Lewandowski, J.-J. Gallet, F. Bournel, M. Rocca, L. Vattuone, Graphene growth on Ni (1 1 1) by CO exposure at near ambient pressure, Chem. Phys. Lett. 774 (2021) 138596, https://doi.org/10.1016/j.cplett.2021.138596.
[33] Z. Novotny, D. Aegerter, N. Comini, B. Tobler, L. Artiglia, U. Maier, T. Moehl, E. Fabbri, T. Huthwelker, T.J. Schmidt, M. Ammann, J.A. van Bokhoven, J. Raabe, J. Osterwalder, Probing the solid–liquid interface with tender x rays: a new ambient-pressure x-ray photoelectron spectroscopy endstation at the Swiss Light Source, Rev. Sci. Instrum. 91 (2020), https://doi.org/10.1063/1.5128600.
[34] M. Smerieri, E. Celasco, G. Carraro, A. Lusuan, J. Pal, G. Bracco, M. Rocca, L. Savio, L. Vattuone, Enhanced chemical reactivity of pristine graphene interacting strongly with a substrate: chemisorbed carbon monoxide on graphene/nickel(1 1 1), ChemCatChem 7 (2015) 2328–2331, https://doi.org/10.1002/cctc.201500279.
[35] Mgr. Jiří libra, KolXPD. https://www.kolibrik.net/en/solutions-products/kolxpd, 2024.
[36] P. Giannozzi, S. Baroni, N. Bonini, M. Calandra, R. Car, C. Cavazzoni, D. Ceresoli, G.L. Chiarotti, M. Cococcioni, I. Dabo, A. Dal Corso, S. de Gironcoli, S. Fabris, G. Fratesi, R. Gebauer, U. Gerstmann, C. Gougoussis, A. Kokalj, M. Lazzeri, L. Martin-Samos, N. Marzari, F. Mauri, R. Mazzarello, S. Paolini, A. Pasquarello, L. Paulatto, C. Sbraccia, S. Scandolo, G. Sclauzero, A.P. Seitsonen, A. Smogunov, P. Umari, R.M. Wentzcovitch, Quantum ESPRESSO: a modular and open-source software project for quantum simulations of materials, J. Phys. Condens. Matter 21 (2009) 395502, https://doi.org/10.1088/0953-8984/21/39/395502.
[37] P. Giannozzi, O. Andreussi, T. Brumme, O. Bunau, M. Buongiorno Nardelli, M. Calandra, R. Car, C. Cavazzoni, D. Ceresoli, M. Cococcioni, N. Colonna, I. Carnimeo, A. Dal Corso, S. de Gironcoli, P. Delugas, R.A. DiStasio, A. Ferretti, A. Floris, G. Fratesi, G. Fugallo, R. Gebauer, U. Gerstmann, F. Giustino, T. Gorni, J. Jia, M. Kawamura, H.-Y. Ko, A. Kokalj, E. Küçükbenli, M. Lazzeri, M. Marsili, N. Marzari, F. Mauri, N.L. Nguyen, H.-V. Nguyen, A. Otero-de-la-Roza, L. Paulatto, S. Poncé, D. Rocca, R. Sabatini, B. Santra, M. Schlipf, A.P. Seitsonen, A. Smogunov, I. Timrov, T. Thonhauser, P. Umari, N. Vast, X. Wu, S. Baroni, Advanced capabilities for materials modelling with Quantum ESPRESSO, J. Phys. Condens. Matter 29 (2017) 465901, https://doi.org/10.1088/1361-648X/aa8f79.
[38] A. Dal Corso, Pseudopotentials periodic table: from H to Pu, Comput. Mater. Sci. 95 (2014) 337–350, https://doi.org/10.1016/j.commatsci.2014.07.043.
[39] I. Hamada, M. Otani, Comparative van der Waals density-functional study of graphene on metal surfaces, Phys. Rev. B 82 (2010) 153412, https://doi.org/10.1103/PhysRevB.82.153412.
[40] K. Lee, É.D. Murray, L. Kong, B.I. Lundqvist, D.C. Langreth, Higher-accuracy van der Waals density functional, Phys Rev B Condens Matter Mater Phys 82 (2010), https://doi.org/10.1103/PhysRevB.82.081101.
[41] I. Lončarić, V. Despoja, Benchmarking van der Waals functionals with noncontact RPA calculations on graphene-Ag(111), Phys. Rev. B 90 (2014) 075414, https://doi.org/10.1103/PhysRevB.90.075414.
[42] S. Patil, D. Perilli, M. Panighel, A. Baby, C. Cepek, G. Comelli, C. Di Valentin, C. Africh, A novel synthesis route with large-scale sublattice asymmetry in boron doped graphene on Ni(111), Surface. Interfac. 51 (2024), https://doi.org/10.1016/j.surfin.2024.104700.
[43] M.G. Cuxart, D. Perilli, S. Tömekce, J. Deyerling, F. Haag, M. Muntwiler, F. Allegretti, C. Di Valentin, W. Auwärter, Spatial segregation of substitutional B atoms in graphene patterned by the moiré superlattice on Ir(111), Carbon N Y 201 (2023) 881–890, https://doi.org/10.1016/j.carbon.2022.09.087.
[44] D. Perilli, D. Selli, H. Liu, E. Bianchetti, C. Di Valentin, H-BN defective layers as giant N-donor macrocycles for Cu adatom trapping from the underlying metal substrate, J. Phys. Chem. C 122 (2018) 23610–23622, https://doi.org/10.1021/acs.jpcc.8b08700.
[45] S. Freddi, D. Perilli, L. Vaghi, M. Monti, A. Papagni, C. Di Valentin, L. Sangaletti, Pushing down the limit of NH3Detection of graphene-based chemiresistive sensors through functionalization by thermally activated tetrazoles dimerization, ACS Nano 16 (2022) 10456–10469, https://doi.org/10.1021/acsnano.2c01095.
[46] S. Fiori, D. Perilli, M. Panighel, C. Cepek, A. Ugolotti, A. Sala, H. Liu, G. Comelli, C. Di Valentin, C. Africh, "Inside out" growth method for high-quality nitrogen-doped graphene, Carbon N Y 171 (2021) 704–710, https://doi.org/10.1016/j.carbon.2020.09.056.
[47] H.J. Monkhorst, J.D. Pack, Special points for Brillouin-zone integrations, Phys. Rev. B 13 (1976) 5188–5192, https://doi.org/10.1103/PhysRevB.13.5188.
[48] K. Momma, F. Izumi, *VESTA 3* for three-dimensional visualization of crystal, volumetric and morphology data, J. Appl. Crystallogr. 44 (2011) 1272–1276, https://doi.org/10.1107/S0021889811038970.
[49] G. Henkelman, A. Arnaldsson, H. Jónsson, A fast and robust algorithm for Bader decomposition of charge density, Comput. Mater. Sci. 36 (2006) 354–360, https://doi.org/10.1016/j.commatsci.2005.04.010.
[50] G. Henkelman, B.P. Uberuaga, H. Jónsson, A climbing image nudged elastic band method for finding saddle points and minimum energy paths, J. Chem. Phys. 113 (2000) 9901–9904.
[51] S. García-Gil, A. García, P. Ordejón, Calculation of core level shifts within DFT using pseudopotentials and localized basis sets, Eur. Phys. J. B 85 (2012) 239, https://doi.org/10.1140/epjb/e2012-30334-5.
[52] M. Wei, Q. Fu, Y. Yang, W. Wei, E. Crumlin, H. Bluhm, X. Bao, Modulation of surface chemistry of CO on Ni(111) by surface graphene and carbidic carbon, J. Phys. Chem. C 119 (2015) 13590–13597, https://doi.org/10.1021/acs.jpcc.5b01395.
[53] F. Späth, K. Gotterbarm, M. Amende, U. Bauer, C. Gleichweit, O. Höfert, H.-P. Steinrück, C. Papp, Keeping argon under a graphene lid—argon intercalation between graphene and nickel(111), Surf. Sci. 643 (2016) 222–226, https://doi.org/10.1016/j.susc.2015.05.009.

[54] R.S. Weatherup, H. Amara, R. Blume, B. Dlubak, B.C. Bayer, M. Diarra, M. Bahri, A. Cabrero-Vilatela, S. Caneva, P.R. Kidambi, M.-B. Martin, C. Deranlot, P. Seneor, R. Schloegl, F. Ducastelle, C. Bichara, S. Hofmann, Interdependency of subsurface carbon distribution and graphene–catalyst interaction, J. Am. Chem. Soc. 136 (2014) 13698–13708, https://doi.org/10.1021/ja505454v.

[55] Y. Dedkov, W. Klesse, A. Becker, F. Späth, C. Papp, E. Voloshina, Decoupling of graphene from Ni(111) via formation of an interfacial NiO layer, Carbon N Y 121 (2017) 10–16, https://doi.org/10.1016/j.carbon.2017.05.068.

[56] S. Uhlenbrockt, C. Scharfschwerdtt, M. Neumannt, H.-J. Freund, The Influence of Defects on the Ni 2p and 0 1s XPS of NiO, 1992.

[57] M. Pozzo, T. Turrini, L. Bignardi, P. Lacovig, D. Lizzit, E. Tosi, S. Lizzit, A. Baraldi, D. Alfè, R. Larciprete, Interplay among hydrogen chemisorption, intercalation, and bulk diffusion at the graphene-covered Ni(111) crystal, J. Phys. Chem. C 127 (2023) 6938–6947, https://doi.org/10.1021/acs.jpcc.3c00291.

[58] D. Lizzit, M.I. Trioni, L. Bignardi, P. Lacovig, S. Lizzit, R. Martinazzo, R. Larciprete, Dual-Route hydrogenation of the graphene/Ni interface, ACS Nano 13 (2019) 1828–1838, https://doi.org/10.1021/acsnano.8b07996.

[59] M. Wijzenbroek, D. Helstone, J. Meyer, G.-J. Kroes, Dynamics of H2 dissociation on the close-packed (111) surface of the noblest metal: H2 + Au(111), J. Chem. Phys. 145 (2016) 144701.

[60] M.M.S. Abdelnabi, C. Izzo, E. Blundo, M.G. Betti, M. Sbroscia, G. Di Bella, G. Cavoto, A. Polimeni, I. García-Cortés, I. Rucandio, A. Moroño, K. Hu, Y. Ito, C. Mariani, Deuterium adsorption on free-standing graphene, Nanomaterials 11 (2021) 130, https://doi.org/10.3390/nano11010130.

[61] I. Di Bernardo, G. Avvisati, C. Chen, J. Avila, M.C. Asensio, K. Hu, Y. Ito, P. Hines, J. Lipton-Duffin, L. Rintoul, N. Motta, C. Mariani, M.G. Betti, Topology and doping effects in three-dimensional nanoporous graphene, Carbon N Y 131 (2018) 258–265, https://doi.org/10.1016/j.carbon.2018.01.076.

[62] A. Nikitin, H. Ogasawara, D. Mann, R. Denecke, Z. Zhang, H. Dai, K. Cho, A. Nilsson, Hydrogenation of single-walled carbon nanotubes, Phys. Rev. Lett. 95 (2005) 225507, https://doi.org/10.1103/PhysRevLett.95.225507.

[63] W. Zhao, J. Gebhardt, F. Späth, K. Gotterbarm, C. Gleichweit, H. Steinrück, A. Görling, C. Papp, Reversible hydrogenation of graphene on Ni(111)—synthesis of "graphone,", Chem. Eur J. 21 (2015) 3347–3358, https://doi.org/10.1002/chem.201404938.

[64] M.G. Betti, E. Blundo, M. De Luca, M. Felici, R. Frisenda, Y. Ito, S. Jeong, D. Marchiani, C. Mariani, A. Polimeni, M. Sbroscia, F. Trequattrini, R. Trotta, Homogeneous spatial distribution of deuterium chemisorbed on free-standing graphene, Nanomaterials 12 (2022) 2613, https://doi.org/10.3390/nano12152613.

[65] D. Degerman, P. Lömker, C.M. Goodwin, M. Shipilin, F. García-Martínez, C. Schlueter, A. Nilsson, P. Amann, State of the surface during CO hydrogenation over Ni(111) and Ni(211) probed by operando X-ray photoelectron spectroscopy, J. Phys. Chem. C 127 (2023) 4021–4032, https://doi.org/10.1021/acs.jpcc.2c07650.

[66] Q.Y. Yang, K.J. Maynard, A.D. Johnson, S.T. Ceyer, The structure and chemistry of CH3 and CH radicals adsorbed on Ni(111), J. Chem. Phys. 102 (1995) 7734–7749, https://doi.org/10.1063/1.469026.

[67] Y. Zang, J. Cai, Y. Han, H. Wu, W. Zhu, S. Shi, H. Zhang, Y. Ran, F. Yang, M. Ye, B. Yang, Y. Li, Z. Liu, CO $_2$ activation on Ni(111) and Ni(110) surfaces in the presence of hydrogen, J. Phys. Chem. Lett. 14 (2023) 4381–4387, https://doi.org/10.1021/acs.jpclett.3c00790.

[68] R. Karthikeyan, D. Thangaraju, N. Prakash, Y. Hayakawa, Single-step synthesis and catalytic activity of structure-controlled nickel sulfide nanoparticles, CrystEngComm 17 (2015) 5431–5439, https://doi.org/10.1039/C5CE00742A.

[69] B. Quan, S.-H. Yu, D.Y. Chung, A. Jin, J.H. Park, Y.-E. Sung, Y. Piao, Single source precursor-based solvothermal synthesis of heteroatom-doped graphene and its energy storage and conversion applications, Sci. Rep. 4 (2014) 5639, https://doi.org/10.1038/srep05639.

[70] N. Kitakatsu, V. Maurice, C. Hinnen, P. Marcus, Surface hydroxylation and local structure of NiO thin films formed on Ni(111), Surf. Sci. 407 (1998) 36–58, https://doi.org/10.1016/S0039-6028(98)00089-2.

[71] S. Goler, C. Coletti, V. Tozzini, V. Piazza, T. Mashoff, F. Beltram, V. Pellegrini, S. Heun, Influence of graphene curvature on hydrogen adsorption: toward hydrogen storage devices, J. Phys. Chem. C 117 (2013) 11506–11513, https://doi.org/10.1021/jp4017536.

[72] J.J. Yeh, I. Lindau, Atomic subshell photoionization cross sections and asymmetry parameters: $1 \leqslant Z \leqslant 103$, At Data Nucl Data Tables 32 (1985) 1–155, https://doi.org/10.1016/0092-640X(85)90016-6.

[73] M.C. Biesinger, Nickel. https://www.xpsfitting.com/2012/01/nickel.html, 2012.

[74] A.P. Grosvenor, M.C. Biesinger, R.StC. Smart, N.S. McIntyre, New interpretations of XPS spectra of nickel metal and oxides, Surf. Sci. 600 (2006) 1771–1779, https://doi.org/10.1016/j.susc.2006.01.041.

[75] M. Caffio, B. Cortigiani, G. Rovida, A. Atrei, C. Giovanardi, Early stages of NiO growth on Ag(001): a study by leis, XPS, and leed, J. Phys. Chem. B 108 (2004) 9919–9926, https://doi.org/10.1021/jp037805o.

[76] G.T. Tyuliev, K.L. Kostov, XPS/HREELS study of NiO films grown on Ni(111), Phys. Rev. B 60 (1999) 2900–2907, https://doi.org/10.1103/PhysRevB.60.2900.

[77] Z. Feng, T. Guohua, Structure sensitivity in hydrogen adsorption on Ni/NiO interfaces for the hydrogen evolution reaction, J. Phys. Chem. C 127 (2023) 23180–23188, https://doi.org/10.1021/acs.jpcc.3c05321.